Theoretical Notes

Note 317

12 January 1981

Coaxial Geometry Experiments

C. Mallon, R. Denson, R. E. Leadon, and T. M. Flanagan

JAYCOR
San Diego, California 92138

TABLE OF CONTENTS

LIST OF ILLUSTRATIONS

SECTION I

INTRODUCTION

The electrical properties of soil have been of interest for some time, especially since soil often serves as the return conductor for long power or communication lines. Most previous work has emphasized low voltages and low frequency effects. EMP excitation of long lines, however, is frequency dependent and may result in large voltages.

The development of the MX missile ground system has renewed interest in EMP coupling to long lines. This interest has resulted in the need for better definition of certain frequency dependent and nonlinear soil parameters. A number of measurements have thus been recently carried out to determine these electrical properties.

Frequency domain measurements of soil conductivity and dielectric constant were first made for comparison with past work. High voltages were then applied to small samples so that nonlinear breakdown parameters could be measured. Finally, a short section of a coaxial geometry filled with soil was used to investigate transmission line phenomena and large sample breakdown effects. This report describes those coaxial geometry tests.

The goals of these coaxial geometry tests include the following:

1. Measure early-time (high frequency) linear transmission line characteristics of a soil-filled line.
2. Check out transmission line instrumentation concepts.
3. Look for breakdown effects on a large scale coaxial geometry.

Experimental results will be discussed in terms of these goals. The test setup will first be described, while instrumentation details are given in the appendix. The next section discusses linear transmission line characteristics. This is followed by a discussion of high voltage tests.

SECTION II

DESCRIPTION OF TEST SETUP

A schematic of the coaxial geometry test configuration is shown in Figure 1. An inner conductor with a diameter of 1.1 cm was placed along the axis of a larger cylinder (44 cm in diameter). A length of 187 cm of this coaxial geometry was filled with soil from the SDF site at Kirtland AFB.

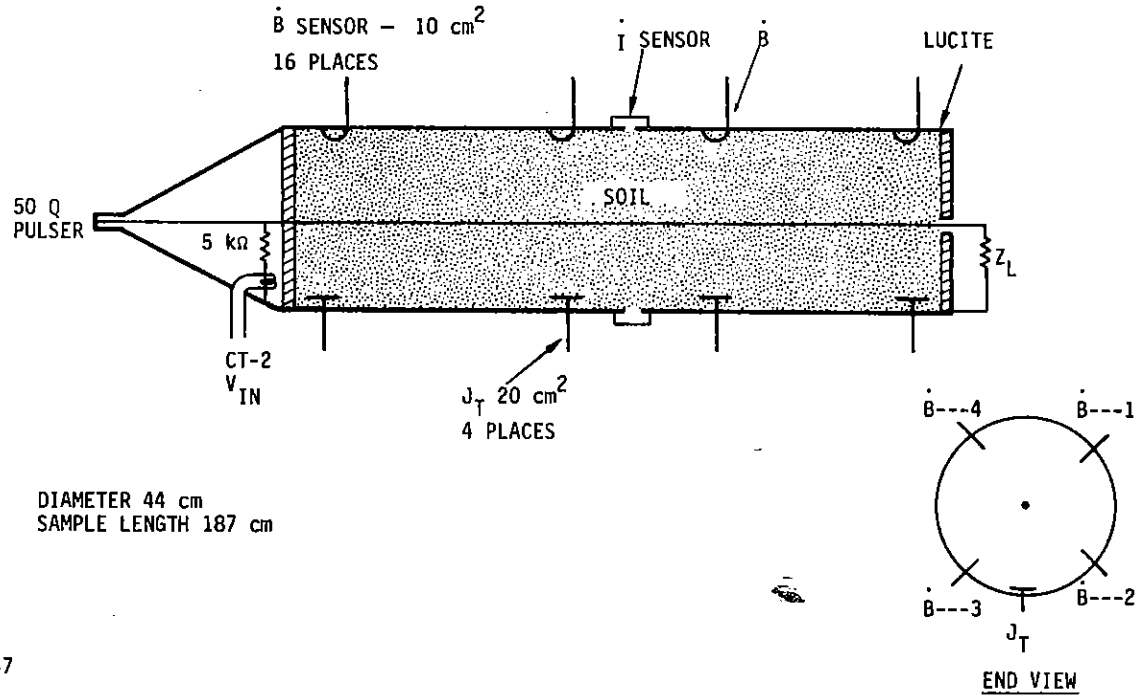

Figure 1. Large volume coaxial chamber

Locations along the coaxial cylinders are indicated in terms of distance, in centimeters, from the lucite plug at the input end of the test object. For example, Station 43 is 43 cm from the beginning of the soil-filled section of the cylinder.

Frequency domain conductivity and dielectric constant measurements were made using small samples of the soil from various locations along the cylinder. These measured parameters are shown for various frequencies in Tables 1 and 2. The electrical properties of the soil appear to be fairly uniform (primarily as a result of thorough mixing of the soil after it arrived). The average soil density was 1.7 g/cm^3 and the water content was about 5.2% (by weight), which is approximately 8.8% by volume.

Table 1

LOW FIELD DATA FOR SAMPLES WITHHELD DURING LOADING OF CYLINDER AND FOR FULLY LOADED CYLINDER

		Dielectric Constant Frequency								
Wt% H_2O	Station	10 MHz	4 MHz	2 MHz	1 MHz	400 kHz	100 kHz	10 kHz	4 kHz	1 kHz
5.1	7	8.8	10.6	11.7	14.0	19.5	43.4	274	625	2.3×10^3
5.3	43	8.6	9.9	11.0	13.0	19.0	42.0	260	612	2.4×10^3
5.8	65	8.9	10.4	11.5	14.0	19.3	42.9	269	615	2.37×10^3
5.0	108	8.7	9.8	11.4	13.5	18.9	42.2	271	595	2.3×10^3
5.1	153	9.2	10.6	13.0	15.6	21.0	63.0	317	736	2.97×10^3
4.9	183	8.5	9.6	11.2	13.0	18.6	40.5	261	612	2.4×10^3
Fully Loaded Cylinder		•	2.5•	6.9	10.4	15.6	34.3	245		

•LCR meter/cylinder resonance between 4 and 10 MHz

Table 2

LOW FIELD DATA FOR SAMPLES WITHHELD DURING LOADING OF CYLINDER AND FOR THE FULLY LOADED CYLINDER

		Conductivity, 10^{-3} (ohm-cm)$^{-1}$ Frequency								
Wt% H_2O	Station•	10 MHz	4 MHz	2 MHz	1 MHz	400 kHz	100 kHz	10 kHz	4 kHz	1 kHz
5.1	7	7.9	6.7	6.2	6.0	5.8	5.6	5.4	5.4	5.3
5.3	43	7.8	6.6	6.3	6.1	5.9	5.8	5.5	5.4	5.3
5.8	65	7.7	6.5	6.1	5.8	5.7	5.5	5.4	5.3	5.2
5.0	108	7.8	6.7	6.2	6.0	5.8	5.7	5.5	5.4	5.3
5.1	153	8.7	7.4	7.1	6.8	6.6	6.4	6.2	6.1	6.0
4.9	183	7.5	6.3	6.0	5.8	5.7	5.5	5.4	5.3	5.2
Loaded Cylinder		4.4	5.7	4.9	4.5	4.3	4.1	4.0		

•Station xx = xx cm from input

Several different types of sensors were installed at different stations along the coaxial geometry. B-dot loops were installed at four stations (7, 59, 125, and 183) on the inside surface of the outer cylinder. Four such sensors were installed azimuthally around the cylinder at each station (to check for azimuthal symmetry). These sensors were oriented so as to measure the azimuthal magnetic field produced by current flow on the center conductor. This current was also monitored by an I-dot sensor which was built into the outer cylinder at station 77. Transverse current densities were measured at four locations (stations 14, 61, 104, and 180) using J-normal sensors. These sensors were near the outer cylinder at the bottom of the test fixture (which was horizontal). The weight of the dirt thus helped insure good contact. A detailed description of each of these sensors is given in the appendix.

Several other sensors were used to measure the input voltage and current. These are also discussed in the appendix. In most cases, the far end of the coaxial geometry was open-circuited. Some data was also recorded with the far end shorted and also resistively terminated.

SECTION III

LINEAR TRANSMISSION LINE CHARACTERISTICS

3.1 INTRODUCTION

The coaxial test geometry forms a short (187 cm) section of soil-filled transmission line. Due to its short length, however, transmission line theory is a reasonable model only at early times (i.e., for times less than several transit times of a pulse along the cylinder). At later times, a simple circuit model is probably more applicable.

A number of fast transient tests were done to investigate the high-frequency transmission line characteristics of the soil-filled coax. A pulser with a very fast rise time (~1 ns) was used to drive the input of the test geometry. Unfortunately, such a fast rise time can be achieved only for rather low voltages (~1 kV). Thus, only linear characteristics of the soil can be determined.

3.2 TRANSMISSION LINE THEORY

Consider a standard transmission line model for a soil-filled coaxial line. Assuming that no magnetic materials are present, the per unit length impedance of the transmission line is purely inductive with

$$L' = \frac{\mu_o}{2\pi} \ell n\left(\frac{r_o}{r_i}\right) \quad . \tag{1}$$

The inductance per unit length, L', depends only on the inner and outer radii (r_i and r_o) of the coaxial conductors.

The transmission line per unit length admittance, Y' consists of parallel conductance and capacitance terms, both of which depend upon soil characteristics and are thus frequency-dependent. In frequency domain (indicated by ~; s is the transform variable)

$$\tilde{Y}' = \tilde{G}' + s\,\tilde{C}' \quad , \tag{2}$$

where

$$\tilde{C}' = \frac{2\pi\tilde{\varepsilon}}{\ell n(r_o/r_i)} \quad , \tag{3}$$

and

$$\tilde{G}' = \frac{2\pi\tilde{\sigma}}{\ell n(r_o/r_i)} \quad . \tag{4}$$

These expressions show the relationship of the transmission line parameters to the frequency-dependent dielectric constant ($\tilde{\varepsilon}$) and conductivity ($\tilde{\sigma}$) of the soil.

The propagation constant, γ, and the characteristic impedance, Z_c, of the transmission line are then given by the standard formulas

$$\gamma = \sqrt{\tilde{Z}'\tilde{Y}'} = \sqrt{s\tilde{L}'(\tilde{G}' + s\tilde{C}')} \tag{5}$$

$$Z_c = \sqrt{\tilde{Z}'/\tilde{Y}'} = \sqrt{sL'/(\tilde{G}' + s\tilde{C}')} \quad . \tag{6}$$

At very high frequencies ($s \to \infty$) it is clear that the sC' term in the admittance dominates the expression for line admittance. One can thus make the high frequency approximations

$$\begin{aligned} \gamma &= \left(s\tilde{L}'\tilde{C}' + s\tilde{L}'\tilde{G}'\right)^{1/2} = \frac{s}{v_\infty}\left(1 + \frac{\tilde{G}'}{\tilde{C}'}\right)^{1/2} \\ &\simeq \frac{s}{v_\infty}\left(1 + 1/2\,\frac{\tilde{G}'}{s\tilde{C}'}\right) \end{aligned} \tag{7}$$

$$\begin{aligned} Z_c &= \left[\frac{\tilde{L}'}{\tilde{C}'}\left(\frac{1}{1 + \tilde{G}'/s\tilde{C}'}\right)\right]^{1/2} \\ &\simeq Z_\infty\left(1 - 1/2\,\frac{\tilde{G}'}{s\tilde{C}'}\right) \end{aligned} \tag{8}$$

where $v_\infty = 1/\sqrt{\tilde{L}'\tilde{C}'}$ = high frequency limit of the velocity of propagation,

and $Z = \sqrt{\tilde{L}'/\tilde{C}'}$ = high frequency limit of the characteristic impedance.

Note that for a semi-infinite line (i.e., for times before reflections occur), the voltage and currents in the line are given by

$$\tilde{V}(z,s) = \tilde{V}(o,s)e^{-\gamma z} \tag{9}$$

$$\tilde{I}(z,s) = \tilde{I}(o,s)e^{-\gamma z} \tag{10}$$

where z is the distance along the line. Also,

$$\frac{\tilde{V}(z,s)}{\tilde{I}(z,s)} = \tilde{Z}_c \tag{11}$$

Thus, a measurement of the voltage and current along the line gives an experimental measure of the characteristic impedance and the propagation constant.

Assume a step function input voltage of magnitude V_o is applied to the input of the line. Then

$$\tilde{V}(z,s) = \frac{V_o}{s} \exp\left(-\frac{s}{v_\infty} + 1/2\ \frac{\tilde{G}'}{v_\infty \tilde{C}'}\right) , \tag{12}$$

which, in time domain, becomes

$$\tilde{V}(z,s) = V_o e^{-\alpha z}\ U\left(t - \frac{z}{v_\infty}\right) , \tag{13}$$

where $U(t - z/v_\infty)$ is a unit step function, and

$$\alpha = 1/2\ \frac{G'}{v_\infty C'} = 1/2\ Z_\infty\ G' \quad .$$

The pulse is thus attenuated (with an attenuation length of α^{-1}) as it propagates down the line at velocity v_∞.

One can also calculate the current pulse along the line to be

$$I(z,t) = \frac{V_o e^{-\alpha z}}{Z_\infty}\left[1 + 1/2\,\frac{G'}{C'}\left(t - \frac{z}{v_\infty}\right)\right] U\left(t - \frac{z}{v_\infty}\right) \qquad (14)$$

By applying a fast voltage pulse to the input of the soil-filled coaxial line, one can thus directly measure the propagation velocity, v_∞, the attenuation, α, and the characteristic impedance, Z_∞. From these and the above expressions, one can calculate σ and ε for the soil, giving a transient measurement of the high-frequency conductivity and dielectric constant. These values can then be compared to the results of small sample CW measurements.

3.3 RESULTS OF FAST RISE TIME TRANSIENT TESTING

A fast rise time ($\lesssim$1 ns) mercury charge-line pulser was used to drive the coaxial line while the various sensors previously mentioned were used to monitor the voltage and current along the line.

As an example, some early-time digitized data showing the current along the line is shown in Figure 2. Figure 2(a) shows the digitized real-time sensor waveforms along the cylinder, and for the B-dot and I-dot sensors their numerically integrated waveforms for the cylinder terminated with 67 ohms. In this figure, the sensor sensitivities has not been folded in. Figure 2(b) is an overlay of the numerical integrals of the B-dot and I-dot sensors with sensor sensitivities included to give early-time center conductor currents along the cylinder. The propagation velocity, v_∞, can be calculated from any pair of early time waveforms. Nine different pairs of waveforms were used to calculate an average propagation velocity of $\tilde{v}_\infty = 1.38 \times 10^8$ m/s, while the standard deviation of the different measurements was 1.5×10^7 m/s.

Note that, from the dimensions of the coaxial geometry, the inductance per unit length is

$$L' \approx 7.3 \times 10^{-7}\ \text{H/m} \quad . \qquad (15)$$

Since $$v_\infty = \sqrt{1/L'C'} \quad , \qquad (16)$$

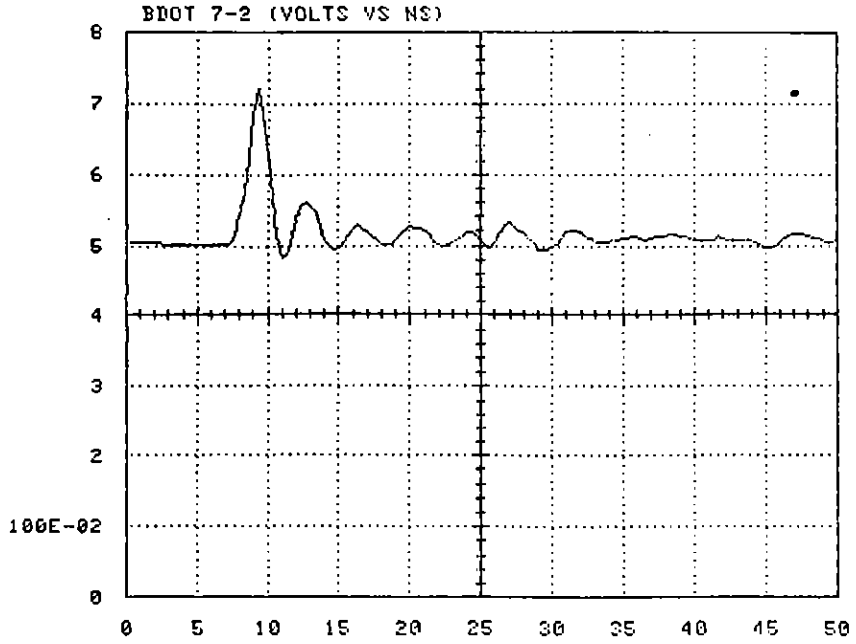

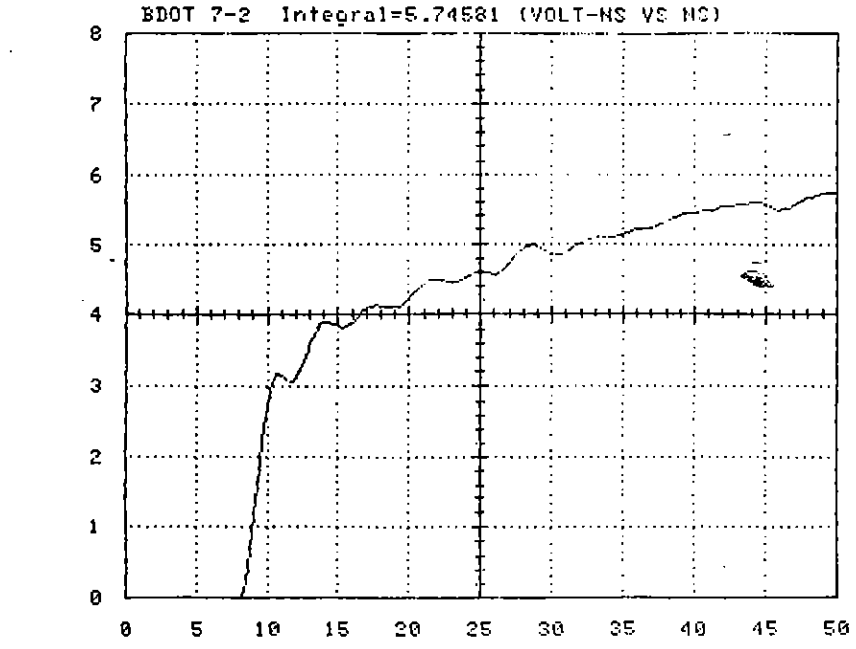

Figure 2(a). Digitized and numerically integrated sensor waveforms along the cylinder for Z_L = 67 ohms (sheet 1 of 7)

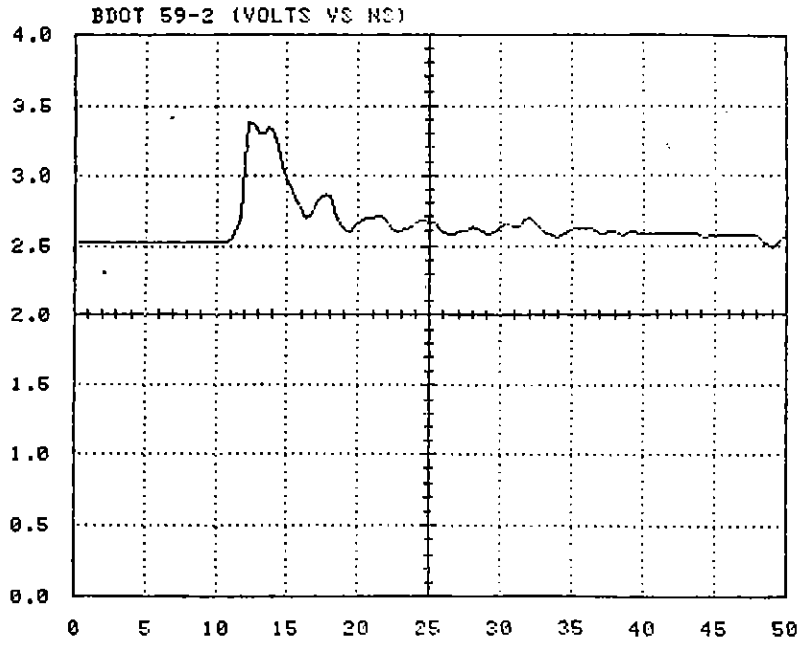

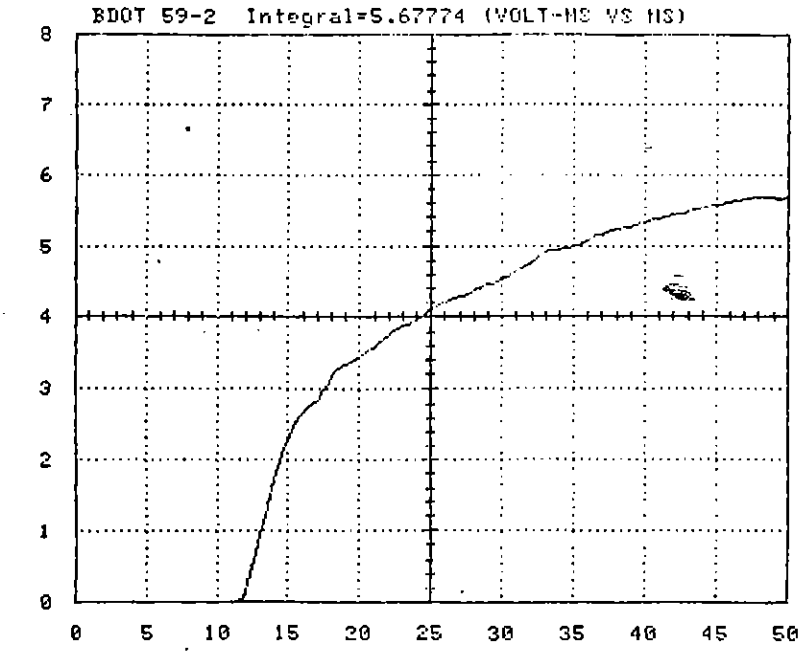

Figure 2(a). Digitized and numerically integrated sensor waveforms along the cylinder for Z_L = 67 ohms (sheet 2 of 7)

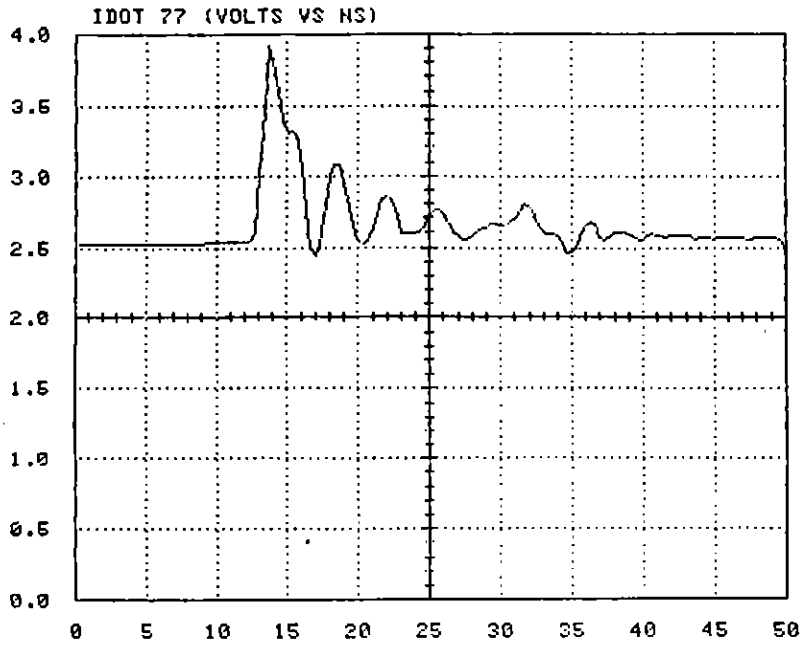

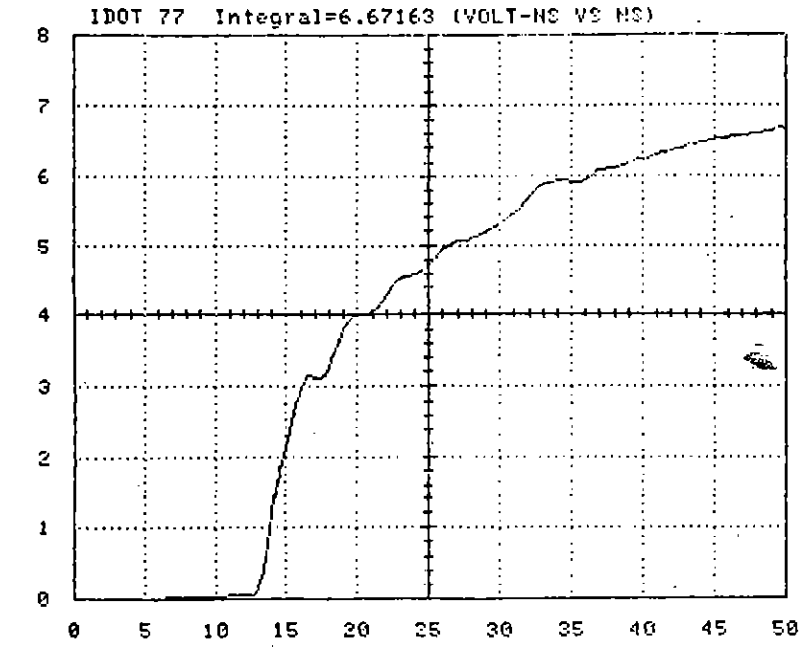

Figure 2(a). Digitized and numerically integrated sensor waveforms along the cylinder for Z_L = 67 ohms (sheet 3 of 7)

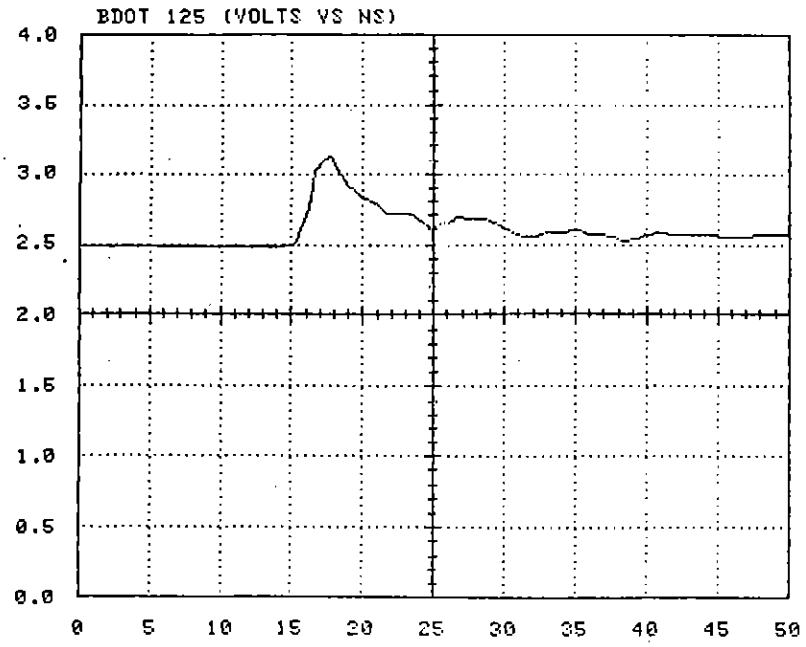

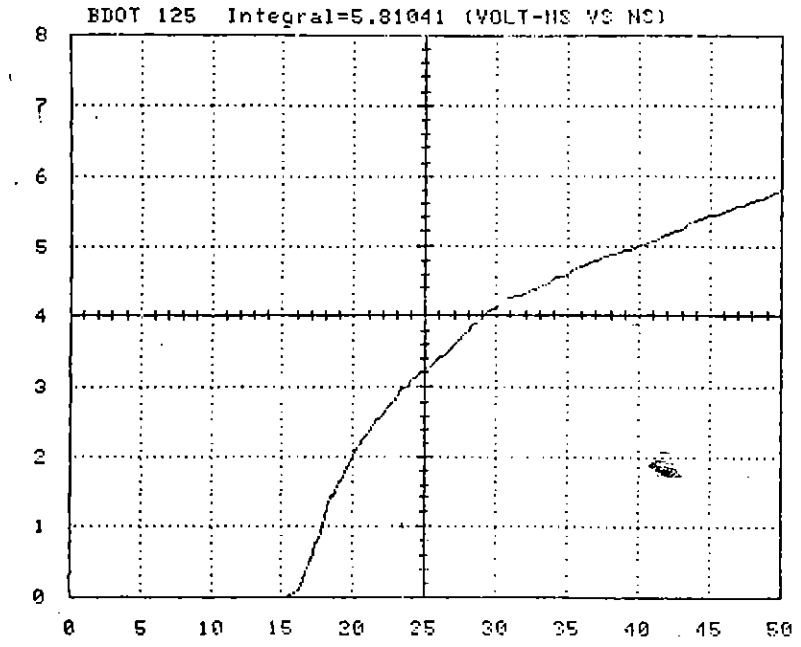

Figure 2(a). Digitized and numerically integrated sensor waveforms along the cylinder for Z_L = 67 ohms (sheet 4 of 7)

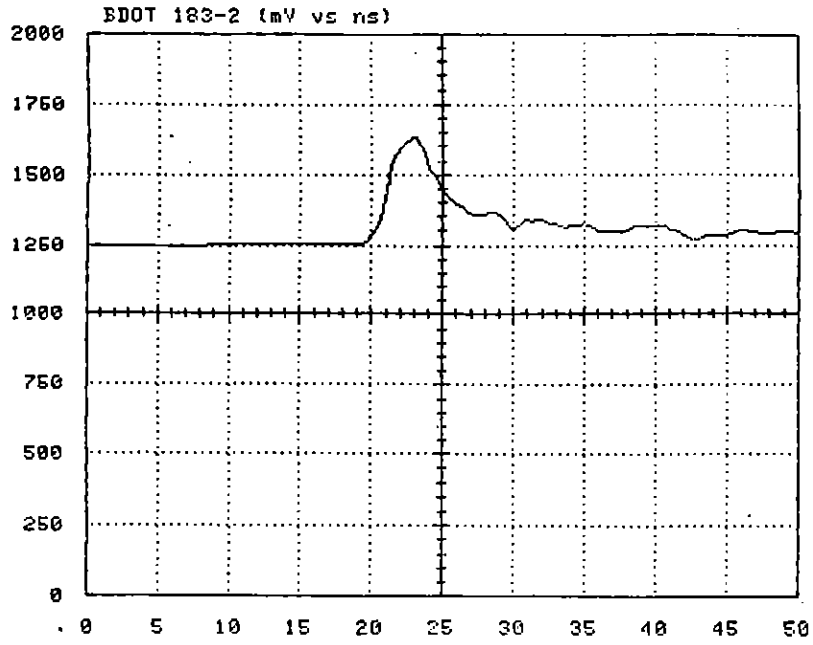

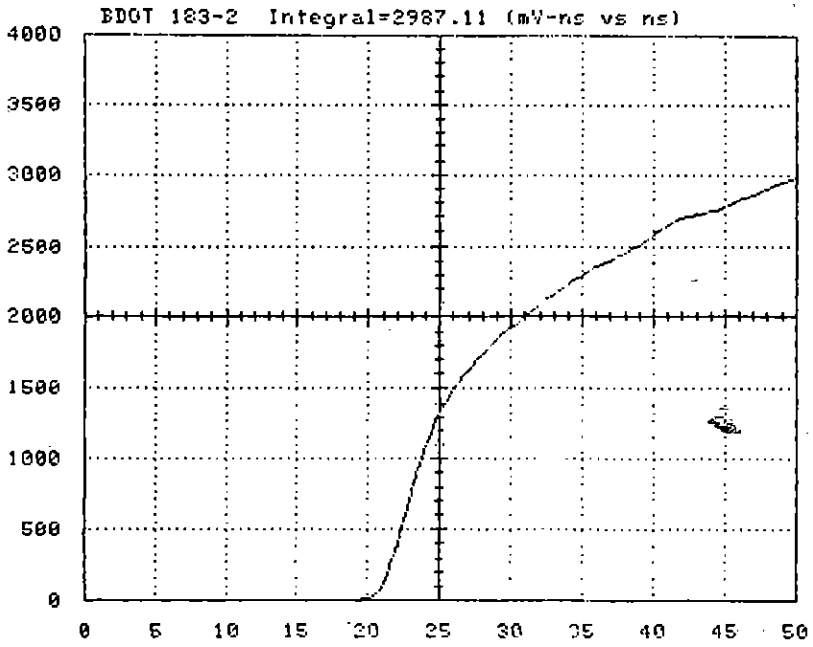

Figure 2(a). Digitized and numerically integrated sensor waveforms along the cylinder for Z_L = 67 ohms (sheet 5 of 7)

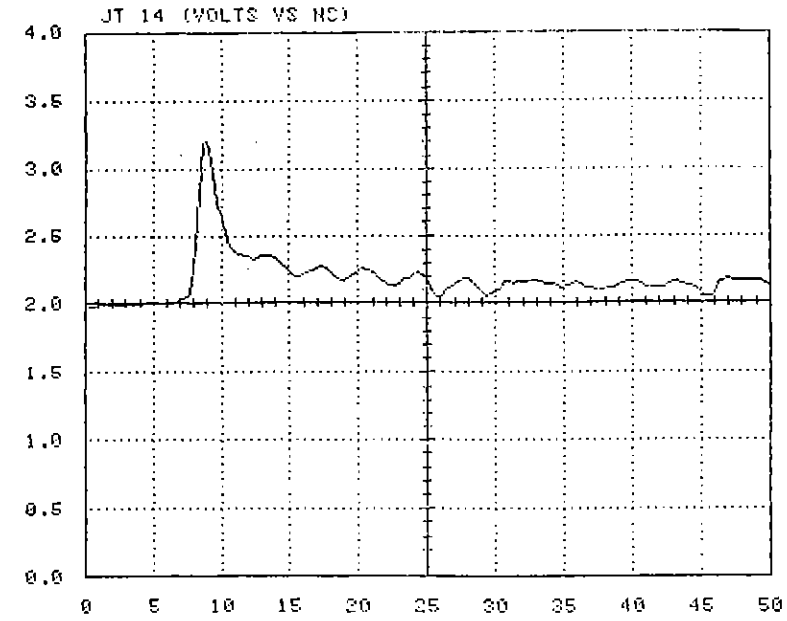

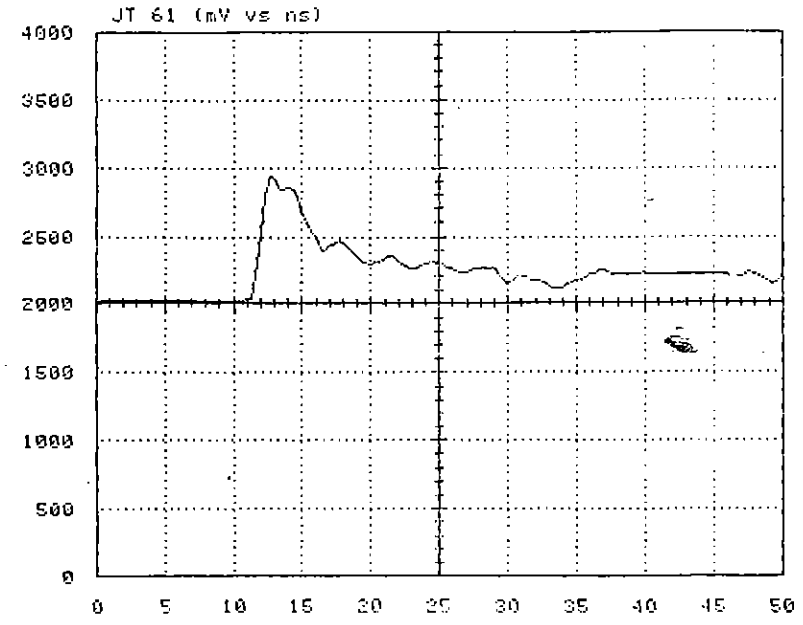

Figure 2(a). Digitized and numerically integrated sensor waveforms along the cylinder for Z_L = 67 ohms (sheet 6 of 7)

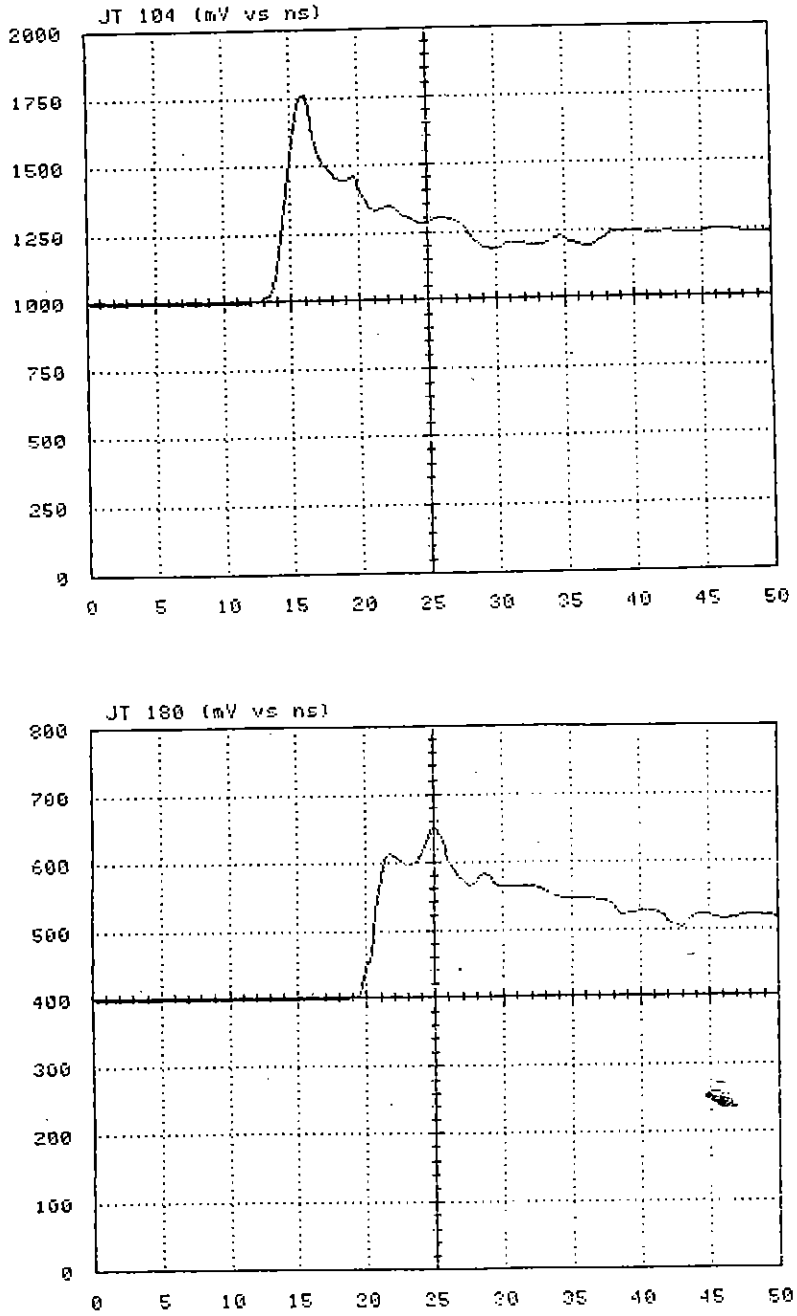

Figure 2(a). Digitized and numerically integrated sensor waveforms along the cylinder for Z_L = 67 ohms (sheet 7 of 7)

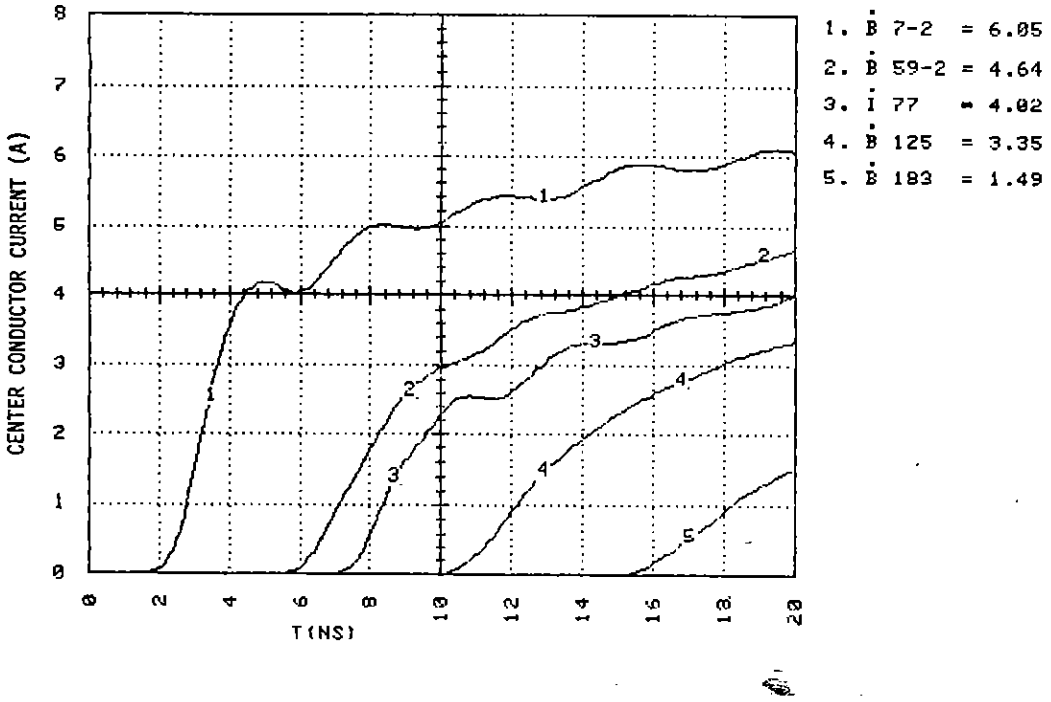

Figure 2(b). Overlay of numerically integrated sensor waveforms along the cylinder scaled to give center conductor current. Z_L = 67 ohms.

one calculates that $C' \simeq 7.2 \times 10^{-11}$ F/m. This implies a relative dielectric constant of $\varepsilon_r = 4.8$. This value is less than any of the small sample CW results shown in Table 1, but the highest frequency in that table is 10 MHz, and ε_r is becoming smaller as frequency increases. The value of the dielectric constant just calculated is thus quite reasonable when one remembers that it is really the high-frequency limit and the upper end of the bandwidth of the transient measuring system being used is several hundred megahertz.

From the calculated inductance and capacitance per unit length one can also find the high-frequency limit of the characteristic impedance, Z_∞. In this case,

$$Z_\infty = \sqrt{\frac{L'}{C'}} \simeq 100.7 \text{ ohms} \quad . \tag{17}$$

One can also determine the decay constant α by examination of the early-time transmission line current waveforms. A calculation of α from five sets of waveforms gives an average value of $\bar{\alpha} = 1.08$ m^{-1} (with a standard deviation of 0.38 m^{-1}). It was shown earlier that

$$\alpha = \frac{Z_\infty G'}{2} \quad , \tag{18}$$

giving

$$G' = 2.1 \times 10^{-2} \text{ mhos/m},$$

and

$$\sigma = \frac{G' \ln(r_o/r_i)}{2\pi} = 1.26 \times 10^{-2} \text{ mhos/m}. \tag{19}$$

A comparison with Table 2 shows that this value of the conductivity is slightly larger than any measured in the small sample CW tests, but the measured conductivity is increasing with frequency and the above conductivity is the high-frequency limit.

The fast rise time transient characteristics of the transmission line can also be described in terms of the reflection coefficient as measured by a TDR. Thus, TDR waveforms for five different termination impedances (Z_L = 0, 50, 67, 100, ∞ ohms) are shown in Figure 3. These waveforms show that the reflection coefficient jumps rapidly at the soil interface to an impedance of about 72 ohms. The reflection coefficient then

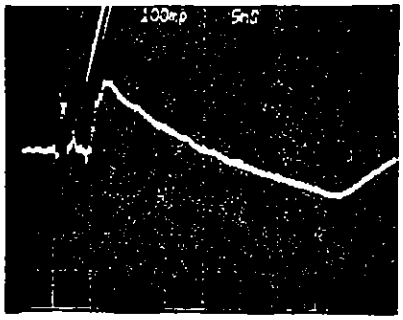

$Z_L = \infty$

100 mρ

5 ns/div

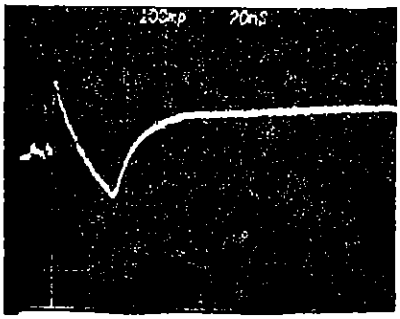

$Z_L = \infty$

100 mρ

20 ns/div

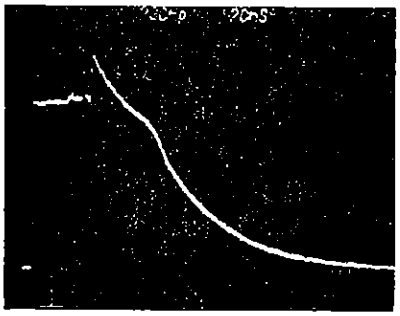

$Z_L = 0$

200 mρ

20 ns/div

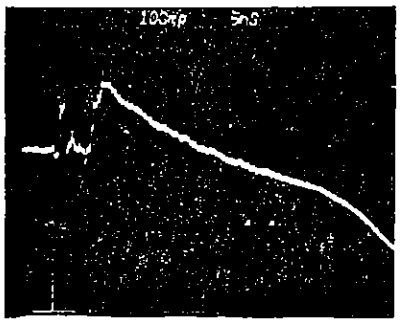

$Z_L = 0$

100 mρ

5 ns/div

Figure 3. TDR waveforms for loaded cylinder for termination impedances, Z_L, of ∞, 0, 100, 67, and 50 ohms (sheet 1 of 3)

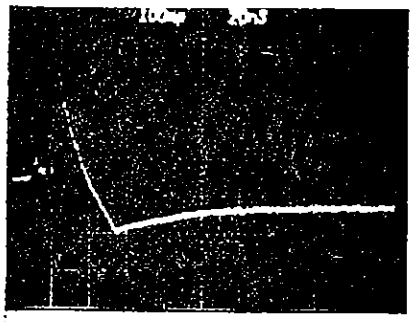

Z_L = 100 Ω
100 mρ
20 ns/div

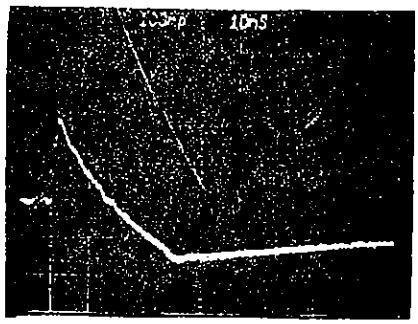

Z_L = 100 Ω
100 mρ
10 ns/div

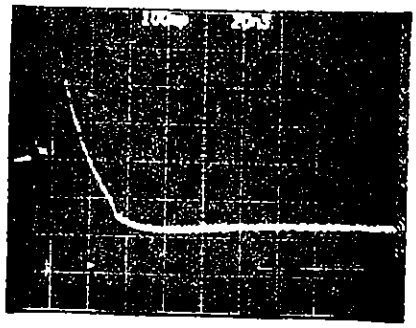

Z_L = 67 Ω
100 mρ
20 ns/div

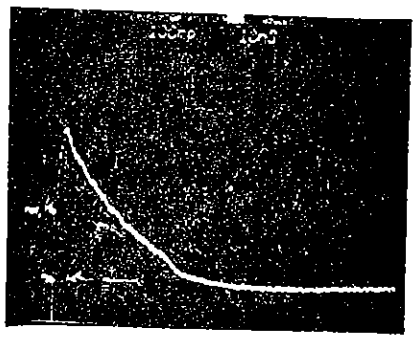

Z_L = 67 Ω
100 mρ
10 ns/div

Figure 3. TDR waveforms for loaded cylinder for termination impedances, Z_L, of ∞, 0, 100, 67, and 50 ohms (sheet 2 of 3)

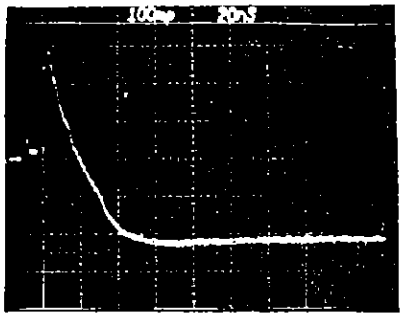

Z_L = 50 Ω

100 mρ

20 ns/div

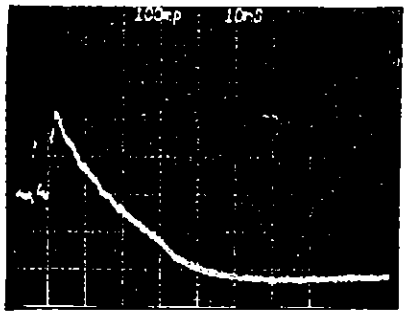

Z_L = 50 Ω

100 mρ

10 ns/div

Figure 3. TDR waveforms for loaded cylinder for termination impedances, Z_L, of ∞, 0, 100, 67, and 50 ohms (sheet 3 of 3)

decreases as the pulse propagates down the line until the end of the line is encountered. Note that a 67 ohm load eliminates any apparent end reflection, while the late-time impedance of an open-circuited line is also about 67 ohms.

3.4 LATE TIME RESULTS

At late times, the coaxial geometry can more easily be thought of as a large coaxial resistor than as a transmission line. For example, if the far end is open, then one expects a constant late-time voltage and a total current depending only on the DC conductivity of the soil.

The fast-rise-time pulser previously referred to has a pulse width of 100 ns, so one can see the various measurements approach late-time, steady-state conditions. Examples of numerous waveforms are shown in Figure 4. The upper trace in Figure 4 is the real-time sensor response and the lower trace shows the integral of the real-time response obtained from a 1.25×10^{-6} s passive integrator. Figure 4 shows the sensor response along the cylinder for the far end terminated in its approximate characteristic impedance of 67 ohms and for the far end open-circuited.

As a specific example, consider the case where the far end of the coaxial test geometry is open-circuited. The ratio of late-time input voltage to input current is then 68 ohms (which agrees quite well with the TDR results). Note that if the soil is assumed to be uniform, the total resistance of the test setup is given by

$$R = \frac{\ell n(r_o/r_i)}{2\pi\ell\sigma} \quad , \tag{20}$$

or

$$\sigma = \frac{\ell n(r_o/r_i)}{2\pi\ell R} \simeq 4.6 \times 10^{-3} \text{ mhos/m} \tag{21}$$

This value of the average conductivity is slightly less than the low-frequency values given in Table 2 for samples withheld during cylinder loading; however, it is in good agreement with LCR data for the fully-loaded cylinder also given in Table 2.

One can also calculate a conductivity from the late-time input voltage and the output of the J-normal sensors (assuming conduction currents dominate at late times). The

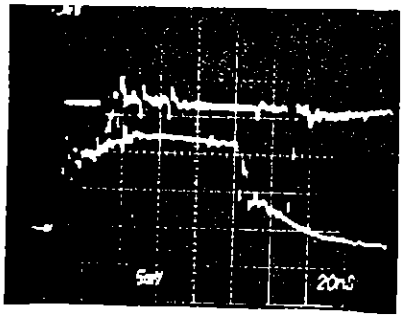

$V_A - V_B$ 6.75 V/Div

$\int V_A - V_B$ 2.32 A/Div

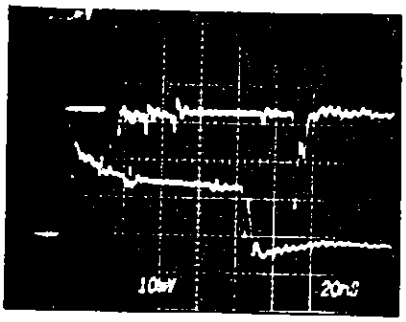

$V_A + V_B$ 13.5 V/Div

$\int V_A + V_B$ 167 V/Div

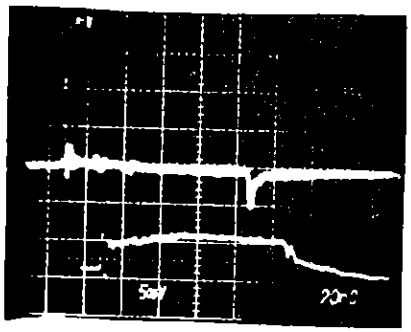

$\dot{B}$ 7-2 1 V/Div

$\int \dot{B}$ 7-2 6.5 A/Div

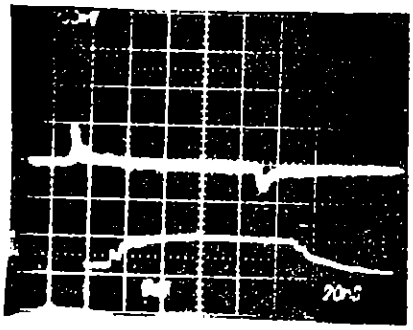

$\dot{B}$ 59-2 1 V/Div

$\int \dot{B}$ 59-2 6.5 A/Div

Figure 4(a). Sensor response to a fast rise time 100 ns pulse. Z_L = 67 ohms, sweep 20 ns/division (sheet 1 of 4)

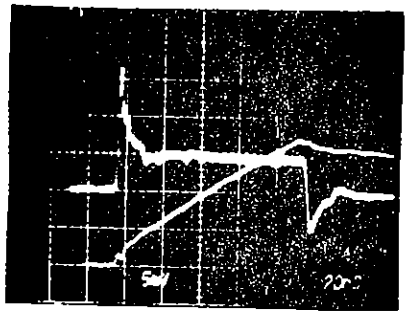

J_T 104 — 5×10^{-3} A/Div

$\int J_T$ 104 — 1.25×10^{-10} Coul/Div.

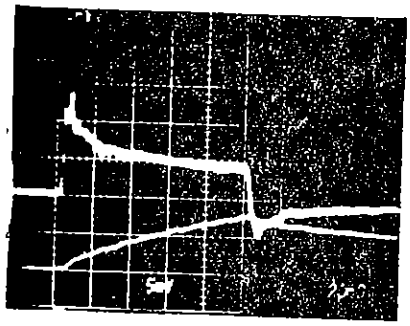

J_T 183 — 2×10^{-3} A/Div

$\int J_T$ 183 — 1.25×10^{-10} Coul/Div

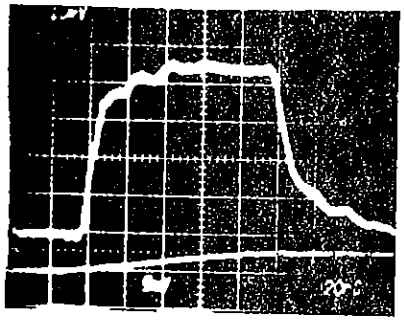

V_{OUT} — CT-2, 49.7 V/Div.

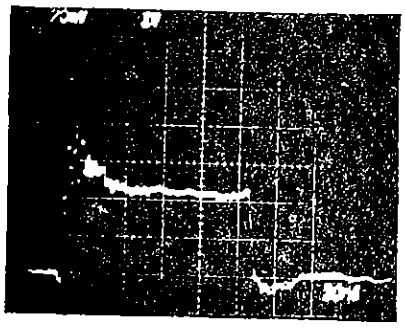

V_{IN} — CT-2, 102 V/Div.

Figure 4(a). Sensor response to a fast rise time 100 ns pulse. Z_L = 67 ohms, sweep 20 ns/division (sheet 2 of 4)

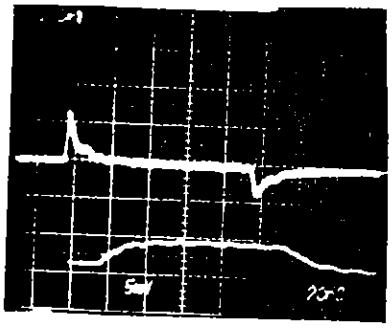

$\dot{B}$ 125-2 0.5 V/Div

$\int \dot{B}$ 125-2 6.5 A/Div

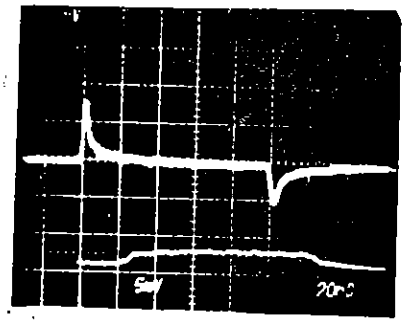

$\dot{B}$ 183-2 0.25 V/Div

$\int \dot{B}$ 183-2 6.5 A/Div

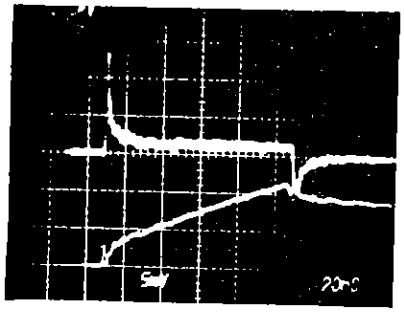

J_T 14 1×10^{-2} A/Div

$\int J_T$ 14 1.25×10^{-10} Coul/Div

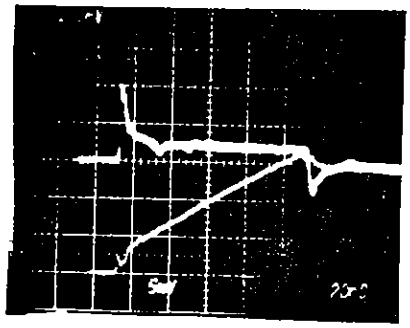

J_T 61 1×10^{-2} A/Div

$\int J_T$ 61 1.25×10^{-10} Coul/Div

Figure 4(a). Sensor response to a fast rise time 100 ns pulse. Z_L = 67 ohms, sweep 20 ns/division (sheet 3 of 4)

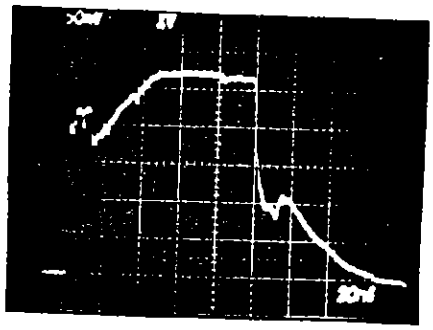

I_{IN} CT-2, 1.25 A/Div.

Figure 4(a). Sensor response to a fast rise time 100 ns pulse. Z_L = 67 ohms, sweep 20 ns/division (sheet 4 of 4)

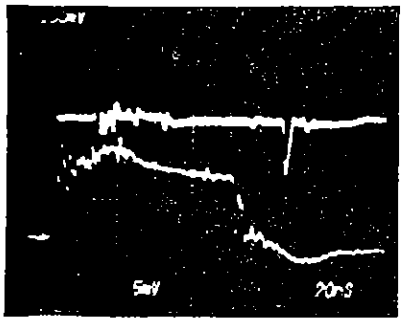

$V_A - V_B$ 13.5 V/Div.

$\int V_A - V_B$ 2.32 A/Div.

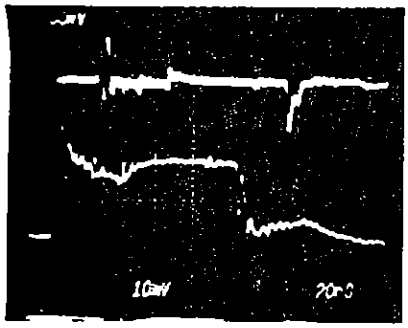

$V_A + V_B$ 2.7 V/Div.

$\int V_A + V_B$ 167 V/Div.

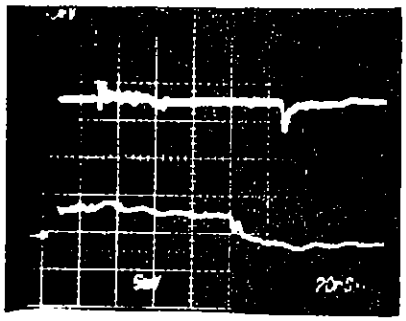

$\dot{B}$ 7.2 1.25 V/Div.

$\int \dot{B}$ 7.2 6.5 A/Div.

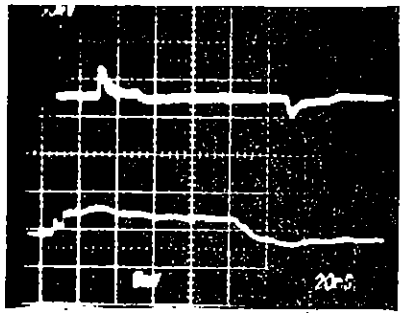

$\dot{B}$ 59-2 1.25 V/Div.

$\int \dot{B}$ 59-2 6.5 A/Div.

Figure 4(b). Sensor response to a fast rise time 100 ns pulse. $Z_L = \infty$, sweep 20 ns/division (sheet 1 of 4)

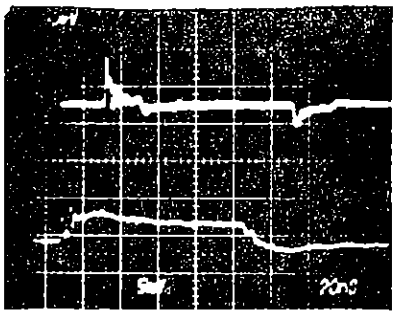

$\dot{I}_{77}$ 1.25 V/Div.

$\int \dot{I}_{77}$ 4.9 A/Div.

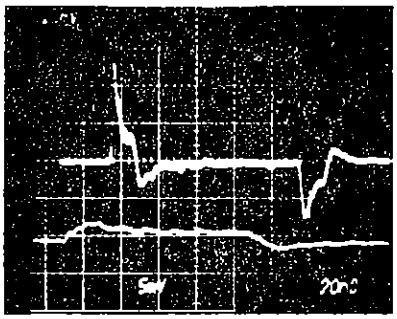

$\dot{B}$ 125-2 0.25 V/Div.

$\int \dot{B}$ 125-2 6.5 A/Div.

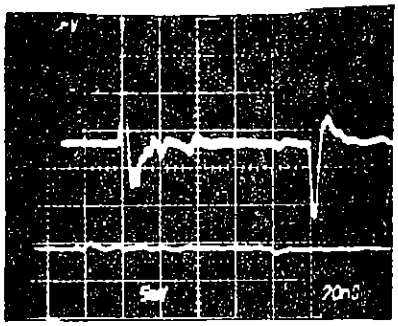

$\dot{B}$ 183-2 0.1 V/Div.

$\int \dot{B}$ 183-2 6.5 A/Div.

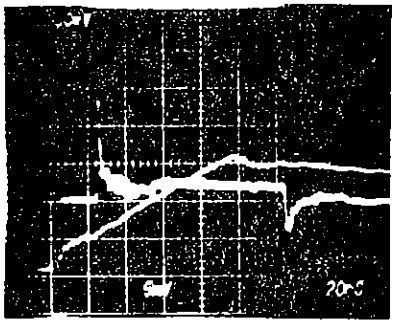

J_T 14 0.01 A/Div.

$\int J_T$ 14 1.25×10^{-10} Coul/Div.

Figure 4(b). Sensor response to a fast rise time 100 ns pulse. $Z_L = \infty$, sweep 20 ns/division (sheet 2 of 4)

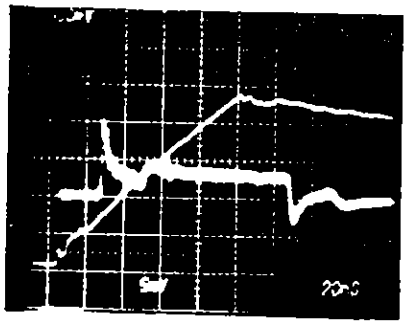

J_T 61 — 0.01 A/Div.

$\int J_T$ 6 — 1.25×10^{-10} Coul/Div.

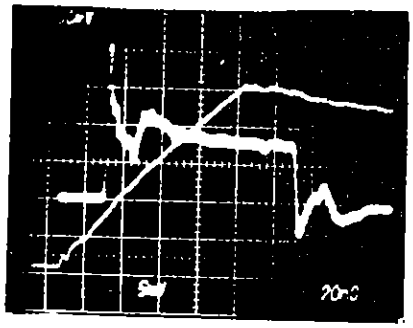

J_T 104 — 4×10^{-3} A/Div.

$\int J_T$ 104 — 1.25×10^{-10} Coul/Div.

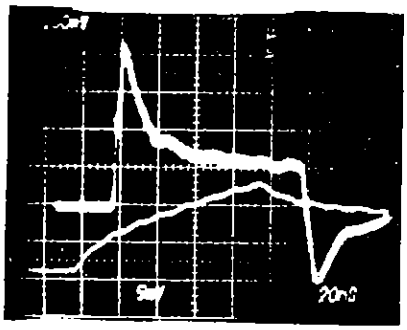

J_T 183 — 2×10^{-3} A/Div.

$\int J_T$ 183 — 1.25×10^{-10} Coul/Div.

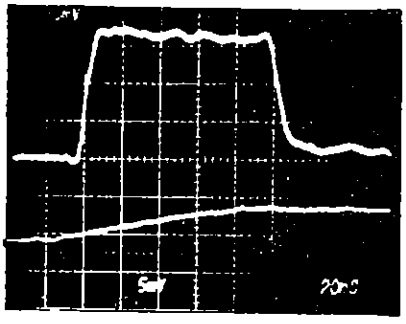

V_{OUT} — CT 2, 99.4 V/Div.

Figure 4(b). Sensor response to a fast rise time 100 ns pulse. $Z_L = \infty$, sweep 20 ns/division (sheet 3 of 4)

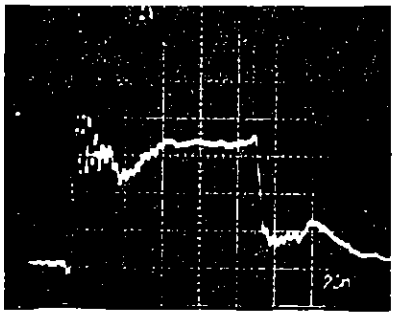

V_{IN} CT-2, 102 V/Div.

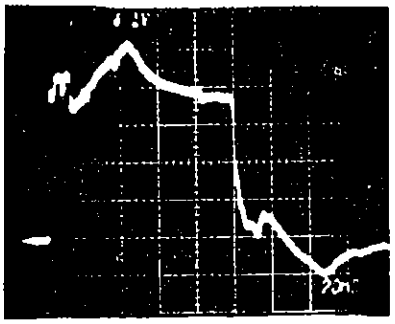

I_{IN} CT-2, 1.25 A/Div.

Figure 4(b). Sensor response to a fast rise time 100 ns pulse. $Z_L = \infty$, sweep 20 ns/division (sheet 4 of 4)

average conductivity calculated from this data is 6.1×10^{-3} mhos/m (and the standard deviation is 1.9×10^{-3} mhos/m). Note that the output of the J-normal sensors vary by up to a factor of two at late times, perhaps indicating either soil nonuniformity or contact resistance differences.

SECTION IV

HIGH VOLTAGE EFFECTS

A high voltage pulser (Pulsar 50 Q) was also used to drive the coaxial test fixture with input voltages of up to about 100 kV. The rise time of this voltage pulser is about 17 ns. A resistive divider was used to vary the peak input voltage. Both drive polarities were also used.

The reason for using a high voltage source is to investigate the possibility of nonlinear soil breakdown effects on a large coaxial geometry. Note that the electric field at a distance r from the axis of the coaxial geometry is given by

$$E(r) = \frac{V_o}{r \ell n(r_o/r_i)} \quad , \tag{22}$$

where V_o = applied voltage
r_i = radius of inner conductor
r_o = radius of outer conductor.

Thus for $V_o = 100$ kV, the electric field at the surface of the inner conductor is

$$E(r = r_i) \simeq 5 \times 10^6 \text{ V/m} \quad .$$

Since small-scale breakdown experiments indicate that the breakdown field for this soil is about 2×10^6 V/m, one would expect breakdown to occur near the inner conductor. On the other hand, the field at the outer electrode is smaller than the breakdown threshold so that arcing all the way between conductors would not be expected.

The measured input current is plotted versus the input voltage in Figure 5. This curve is obviously nearly a straight line, indicating no observable nonlinear behavior that might be attributed to breakdown near the center electrode. Note that changing the polarity of the center electrode has no apparent effect.

Figure 6 shows additional data regarding linearity. This graph plots the center conductor current, as measured by the B-dot loops, per kilovolt of input voltage. The

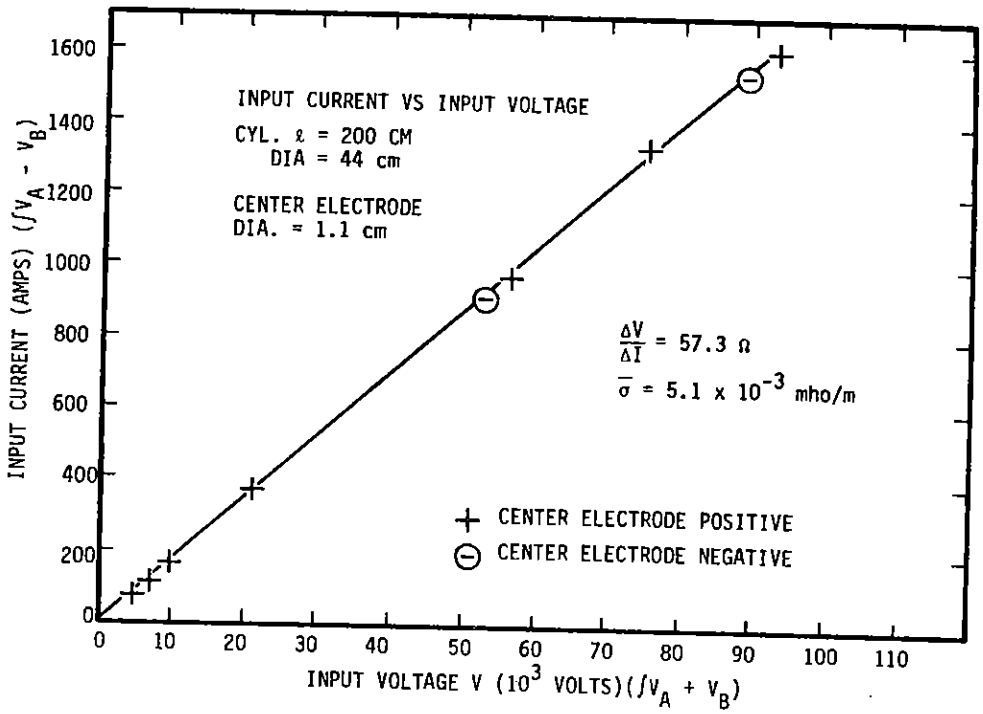

RE-03392

Figure 5. Measured input current versus input voltage for loaded cylinder

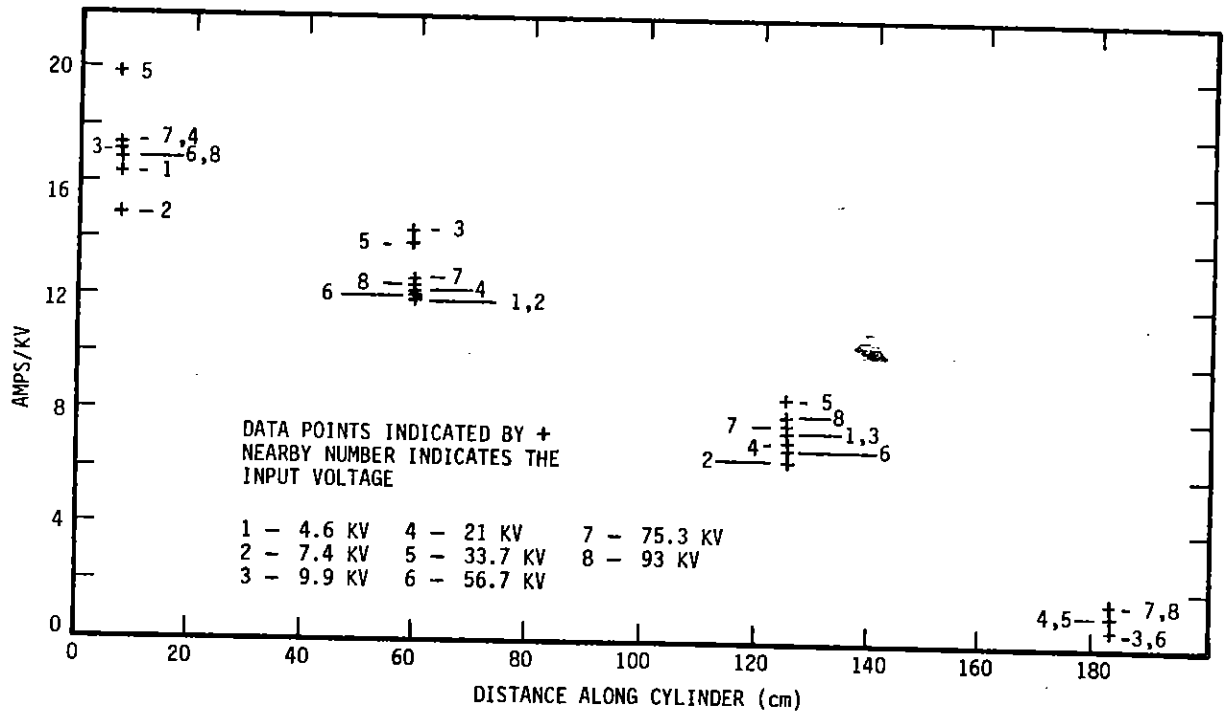

RE-03537

Figure 6. Peak center conductor current per kilovolt of input voltage (as measured by B-dot loops)

input voltage corresponding to individual data points is also indicated. Note that there is some variation in the measured current per kilovolt of input voltage, but the scatter appears to have little correlation with the input voltage. A similar plot is shown in Figure 7 for data from the J-total sensors. Similar results are apparent.

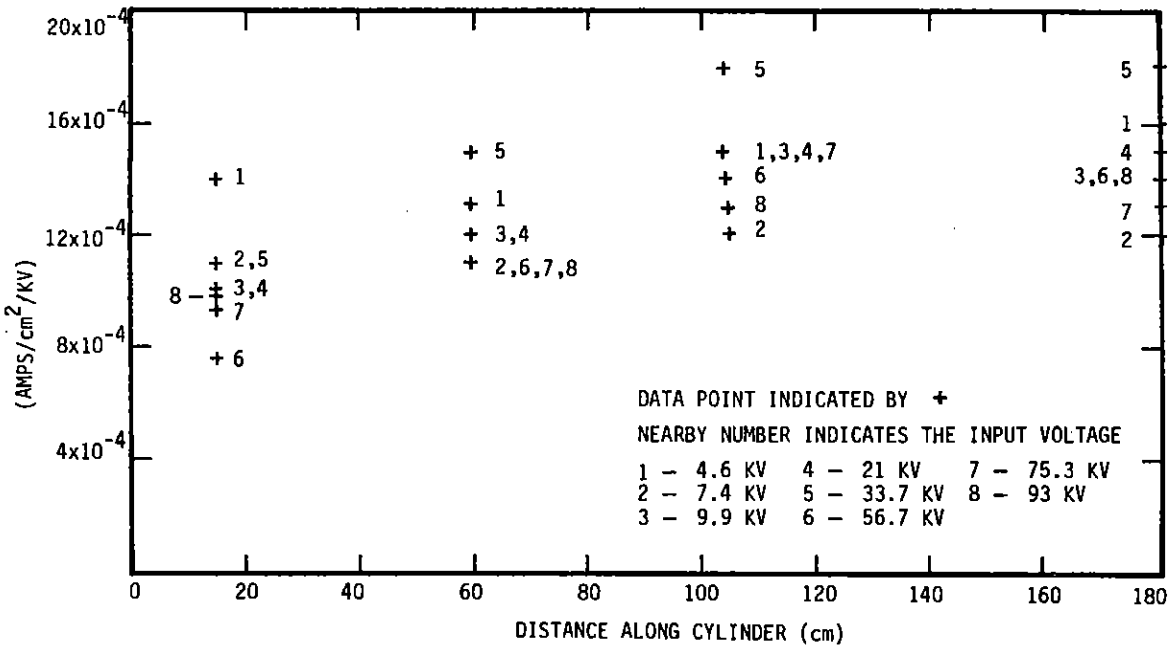

RE-03538

Figure 7. Peak total current density per kilovolt of input voltage (as measured by J-total sensors)

On the basis of such plots and an examination of time domain waveforms, it must be concluded that no clearly nonlinear behavior was observed at high input voltages. One may thus conclude either that no breakdown occurred near the center electrode or that such breakdown effects have a negligible effect on measured parameters.

The $\dot{B}$ sensor located at station 125 ($\dot{B}_{125}$) consistently measured a current approximately 20 percent greater than that expected when compared with $\dot{B}$ and $\dot{I}$ sensors located between stations 7 and 80. At the conclusion of the experiments, inspection of sensor $\dot{B}_{125}$ revealed no sensor problems. This observed over-response may be the result of non-constant soil conductivity along the length of the cylinder. Tables 1 and 2 presented the low-field electrical conductivity and dielectric constant values of soil

samples withheld during loading of the cylinder. The data of Table 2 indicates an increasing conductivity between stations 108 and 153, whereas the conductivity is relatively constant from station 0 to station 108. An increased conductivitiy beyond station 125 would therefore result in a larger relative current at $\dot{B}_{125}$ and a proportionally smaller current at sensor located at the end of the cylinder.

SECTION V

SUMMARY AND CONCLUSIONS

This report has described the results of a series of electrical tests of a short length of coaxial conducting cylinders separated by a region filled with soil. The test geometry is thus a short, soil-filled transmission line.

This coaxial test fixture was instrumented so as to measure the current along the center electrode and the total transverse current density through the soil. When a fast-rise-time pulser was used to drive the test fixture, high-frequency transmission line theory was used to calculate the high-frequency dielectric constant and conductivity of the soil. Results were consistent with small sample CW measurements.

The test fixture was also driven with a high-voltage pulse with the goal of producing breakdown in the soil near the center electrode. No nonlinear effects were observed, however. This indicates the possible need for a larger pulser or a different test geometry in any future experiments.

APPENDIX

DESCRIPTION OF SENSORS

1. B-DOT SENSORS

Cujac-141 cable was used to make simple semicircular B-dot sensors, as shown in Figure 8. The radius of curvature of the loop was 1 inch, giving a loop area of 10.1 cm^2.

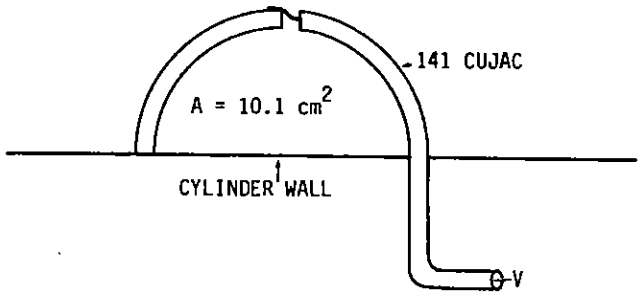

RE-03512

Figure 8. B-dot sensors

Sensor response is given by

$$V_{out} = \dot{B} A \quad , \tag{23}$$

where $\dot{B}$ is the time rate of change of magnetic field through the loop and A is the area. Assuming that the source of magnetic field is the changing current on the center conductor of the coaxial test geometry

$$\dot{B} = \frac{\mu_o \dot{I}}{\pi D} \quad , \tag{24}$$

where D = diameter of outer coaxial cylinder

$\mu_o = 4\pi \times 10^{-7}$ H/m

$\dot{I}$ = rate of change of center conductor current.

Thus, the calibration factor for these sensors is

$$\frac{\dot{I}}{V_{out}} = \frac{\pi D}{\mu_o A} = 1.09 \times 10^{9} \quad \frac{A/s}{V} \quad . \tag{25}$$

Note that the inductance, L, for this semicircular loop is about 4.4×10^{-8} H. The sensor rise time is thus

$$\tau_r = \frac{L}{R} \simeq 8.7 \times 10^{-10} \text{ s} \quad . \tag{26}$$

2. I-DOT SENSORS

A toroidal I-dot sensor, as shown in Figure 9, was built into the outer cylinder of the coaxial test geometry. In this case the output voltage of the sensor is given by

$$V_{out} = M \dot{I} \quad , \tag{27}$$

where $\dot{I}$ = time rate of change of center conductor current

M = mutual inductance

$$= \frac{\mu_o}{2\pi} w \ln\left(\frac{r_o}{r_i}\right) \tag{28}$$

$$\simeq 1.2 \times 10^{-9} \text{ H} \quad .$$

Thus, the calibration factor for this sensor is

$$\frac{\dot{I}}{V_{out}} \simeq 8.3 \times 10^{8} \quad \frac{A/s}{V} \quad . \tag{29}$$

Since the self-inductance of the sensor is approximately equal to the mutual inductance and the output is a 50-ohm cable, the rise time of this sensor is

$$\tau_r = \frac{L}{R} \simeq 2.4 \times 10^{-11} \text{ s} \quad . \tag{30}$$

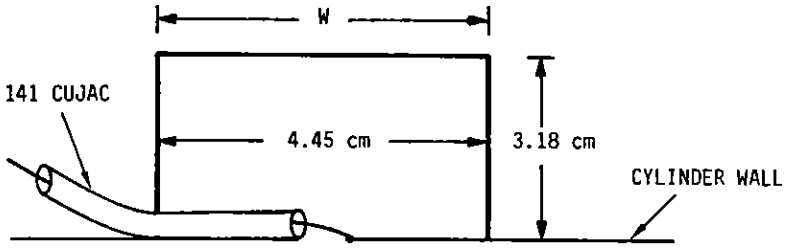

RE-03514

Figure 9. i_{77} sensor

3. J-NORMAL SENSOR

The J-normal sensor, shown in Figure 10, is a circular disk with an area of 20 square centimeters. This disk is attached quite close to the inner surface of the outer cylinder of the coaxial test geometry and connected to the outer cylinder through a 50 ohm load (R_L).

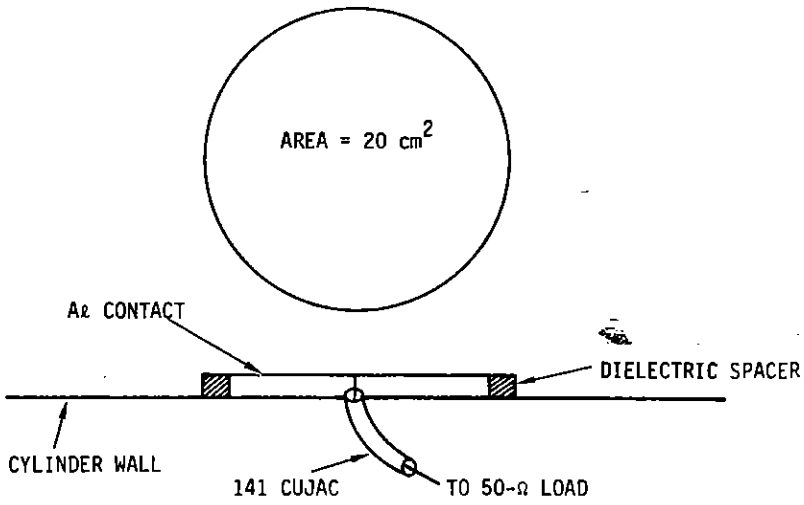

RE-03513

Figure 10. J-total sensors

The output of this sensor is thus given by

$$V_{out} = I_{out} R_L = J_n A R_L \quad , \tag{31}$$

where A = sensor area (20 cm^2)

J_n = transverse current density flowing in the soil between the inner and outer cylinders.

Note that

$$J_n = \varepsilon \frac{\partial E_n}{\partial t} + \sigma E_n \quad , \tag{32}$$

where E_n is the electric field perpendicular to the outer cylinder wall. The sensor thus responds to both displacement and conduction currents.

It may also be useful to remember that the total transverse current per unit length given by a transmission line model is

$$I_T' = C' \frac{\partial V_T}{\partial t} + G' V_T \quad , \tag{33}$$

where V_T = transmission line voltage between coaxial conductors

C' = per unit length capacitance

$$= \frac{2\pi\varepsilon}{\ell n(r_o/r_i)} \tag{34}$$

r_o = radius of outer cylinder

r_i = radius of inner cylinder

G' = per unit length conductance

$$= \frac{2\pi\sigma}{\ell n(r_o/r_i)} \quad . \tag{35}$$

The output current of the J-normal sensor can thus be written as

$$I_{out} = C \frac{\partial V_T}{\partial t} + G V_T \quad , \tag{36}$$

where $$C = \frac{\varepsilon A}{r_o \ell n(r_o/r_i)} \quad , \tag{37}$$

and $$G = \frac{\sigma A}{r_o \ell n(r_o/r_i)} \quad . \tag{38}$$

4. V-DOT/I-DOT SENSOR*

A sensor for measuring the input currents and voltages was also built and attached to the coaxial cable used as an input to the soil-filled test chamber. A diagram of the combined V-dot/I-dot sensor is shown in Figure 11. The sensor was built by cutting two azimuthal slots in the outer shield of RG-17 coaxial line. A larger cylinder is then placed outside the slotted coax and two output cables (50-ohm Cujac) are attached to measure the voltages (V_A and V_B) across the two slots.

The time rate of change of voltage on the inner coaxial line is proportional to the sum of V_A and V_B. This can be seen by noting that a displacement current will flow between the center conductor and the separated segment of cable shield. If the shield-to-center conductor capacitance as denoted by C, this displacement current is $C\dot{V}$. Since the current must then flow across the two gaps,

$$\frac{V_A}{R_L} + \frac{V_B}{R_L} = C\dot{V} = \frac{2\pi\varepsilon(\ell+\Delta)}{\ell n(2b/d)} \tag{39}$$

or

$$V_A + V_B = \frac{2\pi\varepsilon(\ell+\Delta)}{\ell n(2b/d)} R_L \dot{V} \quad , \tag{40}$$

where R_L is the output cable impedance (50 ohms) and the other parameters are identified in Figure 11. In this particular case

$$\frac{\dot{V}}{(V_A + V_B)} = 2.4 \times 10^9 \ \frac{(V/s)}{V} \quad . \tag{41}$$

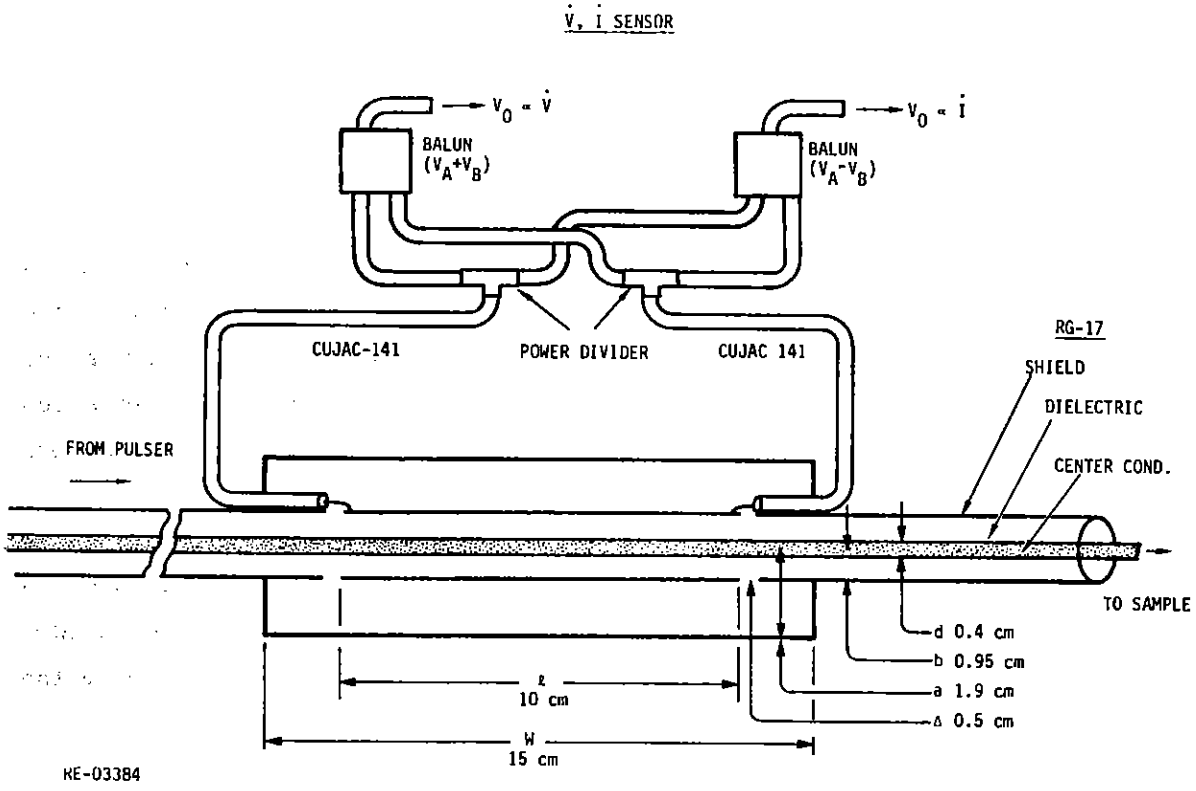

Figure 11. $\dot{V}$-$\dot{I}$ sensor used for coaxial cylinder input voltage and current measurements

On the other hand, the rate of change of center conductor current is proportional to the difference of V_A and V_B. This can be understood by noting the similarity of this sensor's geometry to the more common I-dot sensor. In this case there are two gaps and the output lines are connected so that $V_A - V_B$ is the total voltage along a path around the toroidal cross section formed by the cable shield and the outer conducting cylinder. One thus has

$$V_A - V_B = \int \dot{B}\, dA = M\, \dot{I} \quad , \tag{42}$$

where

$$M = \frac{\mu_o}{2\pi} w\, \ell n(a/b) = 2.1 \times 10^{-8}\ \text{H}. \tag{43}$$

5. INPUT CURRENT AND VOLTAGE

Input current was also measured using a commercial current probe, the CT-2, manufactured by Tektronix. These current measurements were made only during low voltage (~1 kV) fast rise time measurements. Published current probe parameters include:

Sensitivity: 1 V out per A
Rise Time: 0.5×10^{9} s.

Input voltage was also measured by placing four 1000 ohm-2 watt resistors across the input and output, and measuring the current in the resistor by means of the CT-2 probe.